Ridge-like lower mantle structure beneath South Africa

Sidao Ni and Don V. Helmberger
Seismological Laboratory, California Institute of Technology, Pasadena, California, USA

Received 9 October 2001; revised 13 August 2002; accepted 23 October 2002; published 13 February 2003.

[1] Recent (ScS-S) results from probing the deep structure beneath southern Africa display strong delays of up to 10 s at distances beyond 90°. Such delays could be explained by long-period tomographic models containing smooth (weak) features with the addition of rough (strong) D″ structure (3–9% drops in shear velocities). However, these structures cannot explain the (SKS-S) differentials sampling the same region. To explain the (SKS-S) and (ScS-S) data sets simultaneously requires instead a large-scale ridge-like structure with a relatively uniform 3% reduction in shear velocity. The structure is about 1000 km wide and extends at least 1200 km above D″. It is orientated roughly NW-SE and leans toward the east at latitudes from 15° to about 30°. It proves difficult to explain such sharp features with thermal effects alone and, thus, the importance of high-resolution waveform modeling to establish their existence. To derive the above results, we developed a special algorithm by matching simulated synthetics to observed broadband waveforms. This is achieved by computing the various arrivals separately using generalized ray theory for a reference model and allowing the arrivals to shift in relative times to match the data. Tomographic models can then be constructed, or existing tomographic models can be altered, to match these data, and new 2-D synthetics can be constructed as well to better fit the waveform data. These updated synthetics can again be decomposed and reassembled, and the process can be repeated. This algorithm is applied to a combination of analog and digital data along a corridor from South America, producing the high-resolution 2-D model described above. *INDEX TERMS:* 7203 Seismology: Body wave propagation; 7207 Seismology: Core and mantle; 7260 Seismology: Theory and modeling;
KEYWORDS: low velocity structure, Africa, super plume, SKS differential time

Citation: Ni, S., and D. V. Helmberger, Ridge-like lower mantle structure beneath South Africa, *J. Geophys. Res.*, *108*(B2), 2094, doi:10.1029/2001JB001545, 2003.

1. Introduction

[2] The most anomalous large-scale structure in the lower mantle occurs beneath South Africa [*Su et al.*, 1992; *Grand*, 1994; *Masters et al.*, 1996; *Li and Romanowicz*, 1996; *Ritsema et al.*, 1999]. The anomalous geoid signature over Africa is also attributed to this low velocity structure [*Hager et al.*, 1985] as well as for the high elevation of the South African Continent [*Gurnis et al.*, 2000]. To test and enhance these dynamic models requires better 3-D images of the velocity structure, which is presently lacking because of the sparsity of data and our inability to handle the imaging of such severe structures. For example, consider the two tomographic models displayed in Figure 1 along with synthetic seismogram predictions for comparison with a recent published record section, *Wen et al.* [2001]. These two models (GM and RM) have fundamental differences. While GM has a relatively slow basal layer, the other tomographic models listed above have smoother and a more distributed nature. Neither model fits the data although GM is closer because of its slower basal layer. Most long-period tomographic studies use filtered data (periods >20 s) where S and ScS as in Figure 1 appear as one broaden arrival. Thus, such studies become insensitive to the complexity apparent in these observed seismograms where ScS is very delayed.

[3] This record section is particularly interesting in that the ScS at the shortest distance appears to be multipathed (broaden). Features such as this typically appear when phases cross or reflect near an ultralow velocity zone (ULVZ) where two distinctly different paths become available, i.e., *Luo et al.* [2001]. These features are quite apparent in numerical calculations under such conditions as well, *Cormier* [2000]. Note that ScS is probably sampling the ULVZ at the smaller distances as discussed by *Ni and Helmberger* [2001] and indicated in the cross-section (Figure 1). *Wen et al.* [2001] have modeled these records beyond 87° very well by invoking a 200 km basal layer with a greatly reduced velocity. However, such a model is not compatible with other data sets [*Ritsema et al.*, 1998a] along an isolated corridor from Sandwich Island to Tanzania (Figure 2). They find that S is progressively delayed up to 10 s with respect to PREM [*Dziewonski and Anderson*, 1981] at epicentral distances from 60° to 76°, and ScS-S from the data set is about 12 s larger than PREM predictions. Note that the S phase would not be affected by a

0148-0227/03/2001JB001545$09.00

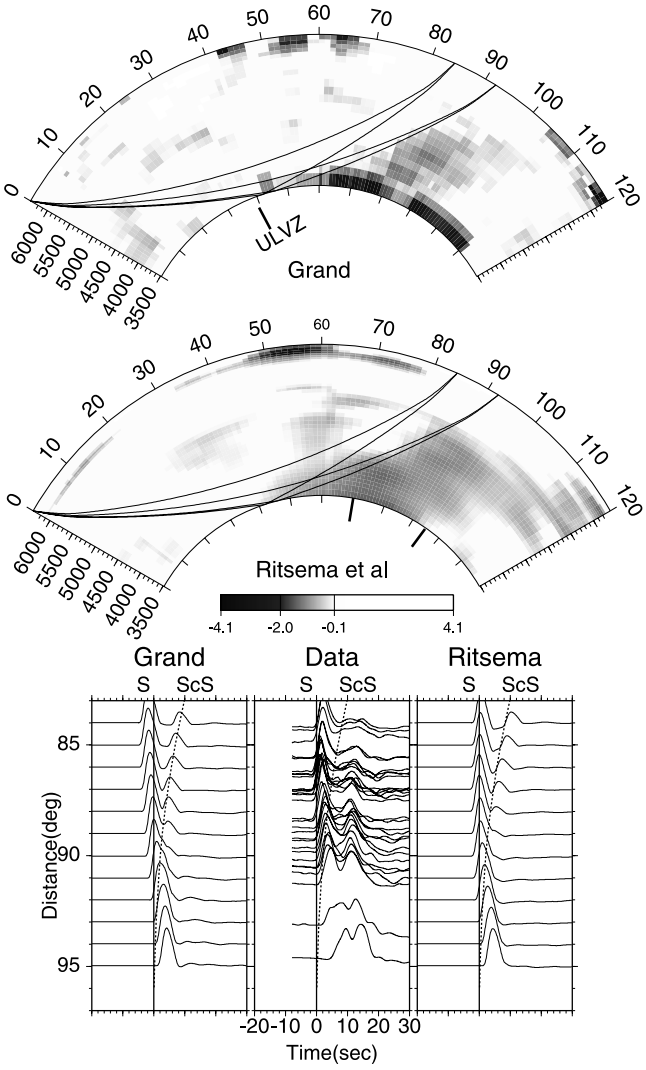

Figure 1. Upper panels contain 2-D sections (tomographic models) by *Grand* [1994] and *Ritsema et al.* [1999] from South Americas to Africa (14°S, 69°W to 28°S, 26°E). We will refer to these models as GM and RM. We have included geometric ray paths for S (light) and SCS (heavy) for distances 84 and 94° to indicate the portion of the core-mantle-boundary (CMB) that is being sampled. The position of an ultralow-velocity zone (ULVZ) is indicated in the upper section and the approximate edges of the Africa Low Velocity Structure (ALVS) is indicated in the second section by heavy bars. The range of velocity variations is given by the grey bar. The lower panels display synthetic seismogram predictions [*Ni et al.*, 2000] generated from these two sections along with observations from the South Africa Array [*Wen et al.*, 2001]. The sections are aligned on the S-wave times predicted by PREM. The corresponding ScS times are given as a dotted line. These data were produced by a deep South America Event (28 November 1997) indicated in Figure 2 by the large star.

simple slow basal layer at these ranges since the bottoming depths of these ray paths are at least 800 km above the core. However, this particular corridor can be explained by introducing a 2-D structure where S samples a longer portion of the slow structure relative to ScS as displayed in Figure 1. Moreover, SKS observations from an event occurring beneath the Drake Passage (tip of South America) features a 10 s delay in SKS arrival between 86 and 92° beyond where the SKS arrival suddenly becomes normal. This jump occurs near the boundary labeled EB in Figure 2. *Ni et al.* [1999] have studied SKS-S crossover distance to constrain the western boundary (WB) of the African Low Velocity Structure (ALVS). Their preliminary results derived from the variation of crossover distance and S to SKS travel times for epicentral distance between 83 and 105 show that there is a low velocity layer (240 km thick or less, with shear velocity reduction about 3%) beneath the Atlantic Ocean which seems to transition sharply into an upwelling beneath western Africa. Their 2-D model is based entirely on analog data (paper records produced by the WWSSN) of the type used in Grand's study, and is essentially in agreement with his results where D″ is considerably slower than the other longer period tomographic features suggest.

[4] A more detailed picture of the transition and the low velocity layer beneath the Atlantic proves difficult to obtain with the data mentioned above for two reasons. On one hand, to model the low velocity layer, the differential time between S and ScS for epicentral distances larger than 87° (where S ray path begins to sample the lower 300 km of the mantle) is crucial. But to measure the separation between S and ScS for the range of epicentral distances is difficult because S and ScS approach each other and this interference makes handpicking of S and ScS arrival difficult (Figure 3). On the other hand, to model the transition of the low velocity layer into ALVS, SKS-S differential times before crossover distances would be helpful since SKS and S ray paths are closer together in the upper mantle, thus more sensitive to lateral variation in D″. But this is difficult too, because of the interference between SKS and S around the crossover distance. For distances of a few degrees before the

Figure 2. (opposite) The top panel (map) displays the locations of deep South American earthquakes and recording stations in Africa. IRIS and WWSSN stations are denoted as squares and array stations by gray triangles. The small, dark triangles located beneath the Atlantic Ocean indicate the ScS bounce points from the array stations with the larger triangles indicating bounce points for the other stations. The dashed lines are approximate edges of the lower mantle ALVS projected on to the CMB. The various paths to the African Array Stations are bracketed by the heavy lines with WB and EB indicating the western and eastern boundaries. The background colors are from Ritsema's tomographic model (basal layer) with maximum reductions of up to 1.5% (golden). The bottom panel indicates the positions of the SKS exit points (diamonds) at the CMB along with station locations. Note that SKS points from LSZ (red) sample the middle of the ALVS while the other paths sample the left boundary (blue and blue-green) and right boundary (green).

(a) Path Geometry

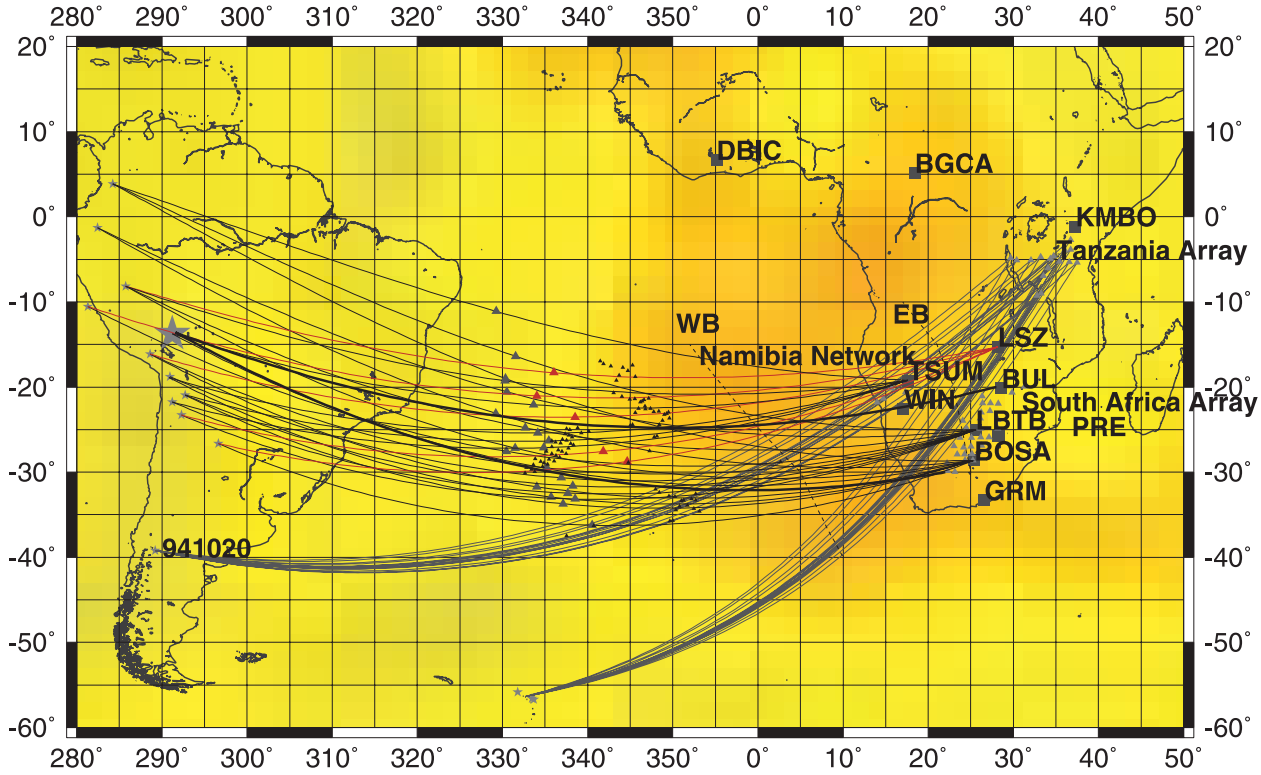

(b) SKS exit points

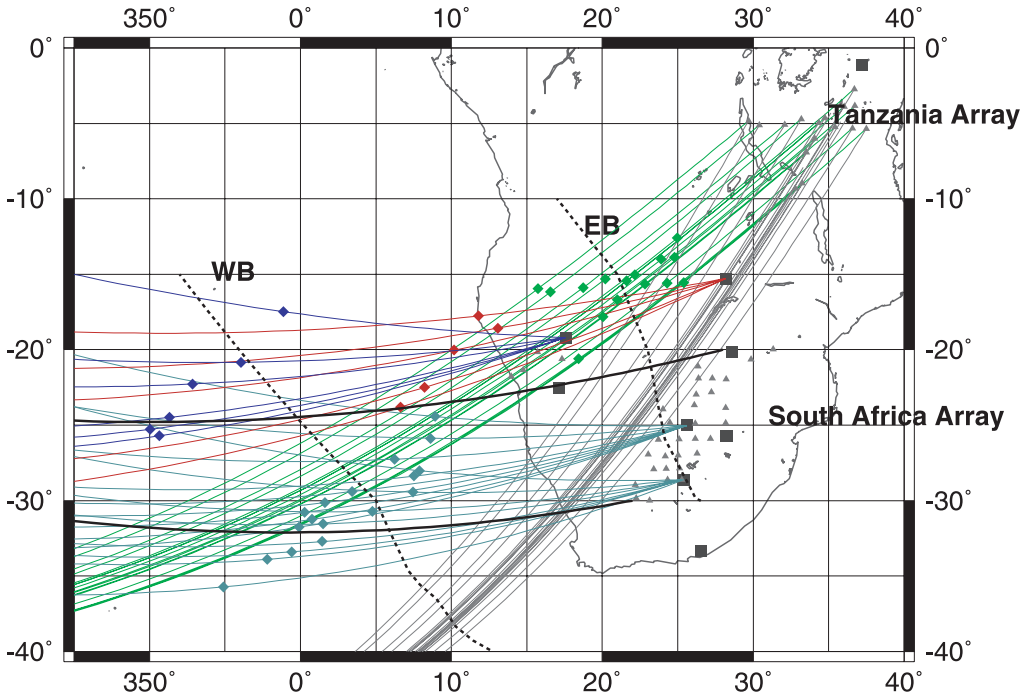

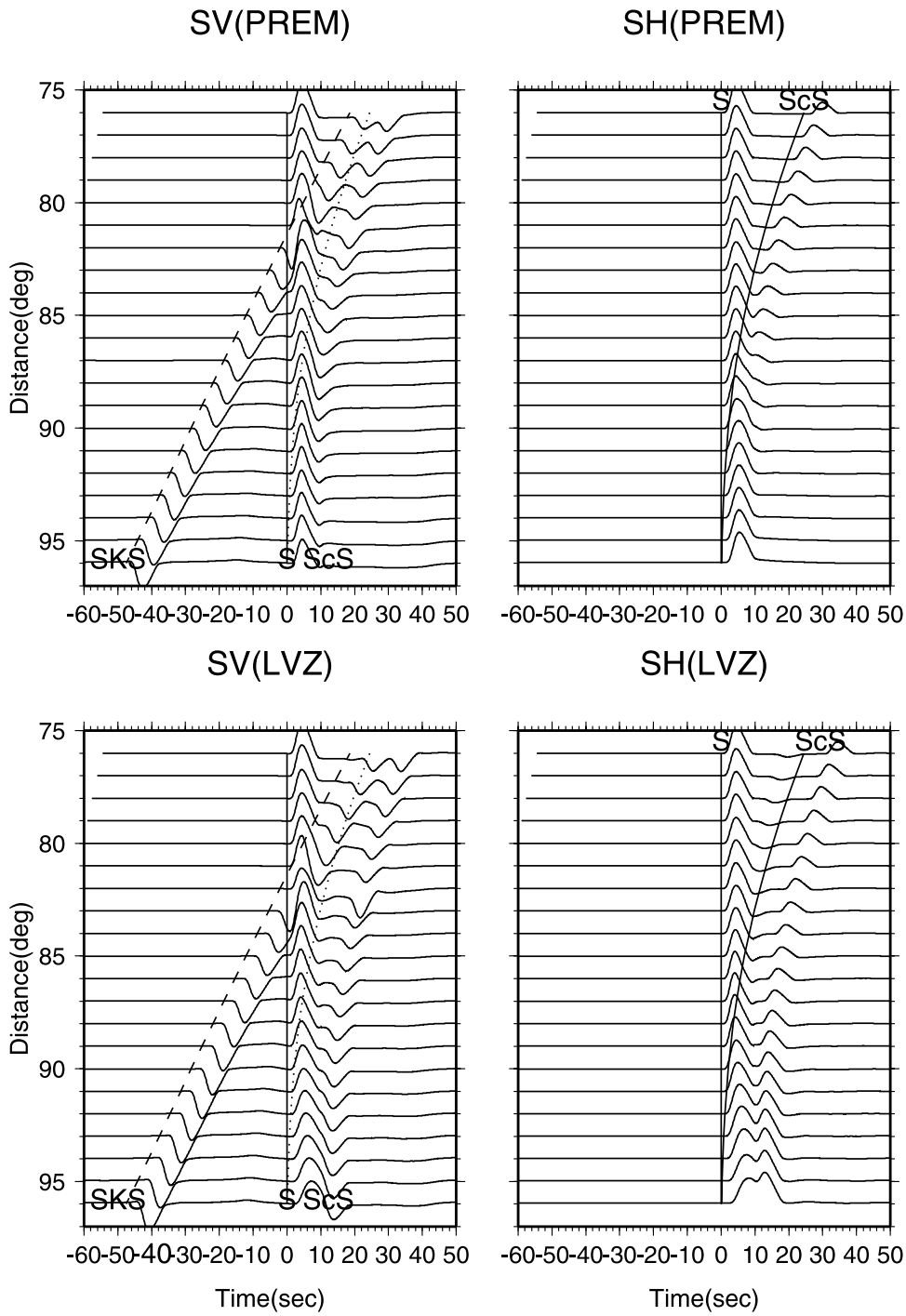

Figure 3. Generalized ray (GRT) synthetic seismograms for PREM and a model containing a low velocity layer (LVZ) above the CMB. The layer is 180 km thick, with a 3% S velocity reduction. Note the crossover distance of SKS to S is about 2° later for the LVZ model than that of PREM, and that S is longer period beyond 93° due to the diffraction caused by the LVZ layer.

crossover distance, SKS is separated from S, but then it begins to interfere with ScS.

[5] Because of difficulties mentioned above, many long-period tomographic studies do not use the SKS data before 90° and ScS+S data beyond 87°. This is especially true for those tomographic studies that determine specific arrivals by correlating a seismic phase from data with seismic arrivals on reference synthetic seismograms because such correlation method does not provide correct results when two seismic phases interfere for complex structures, similar to the case of the SKS-S cross over and the emerging ScS-S. When the epicentral distances become larger than about 95°, the S waveform can be affected by D″ velocity structures. In this case, the differential travel time itself is not sufficient to study the structure, and modeling the whole waveform proves more diagnostic.

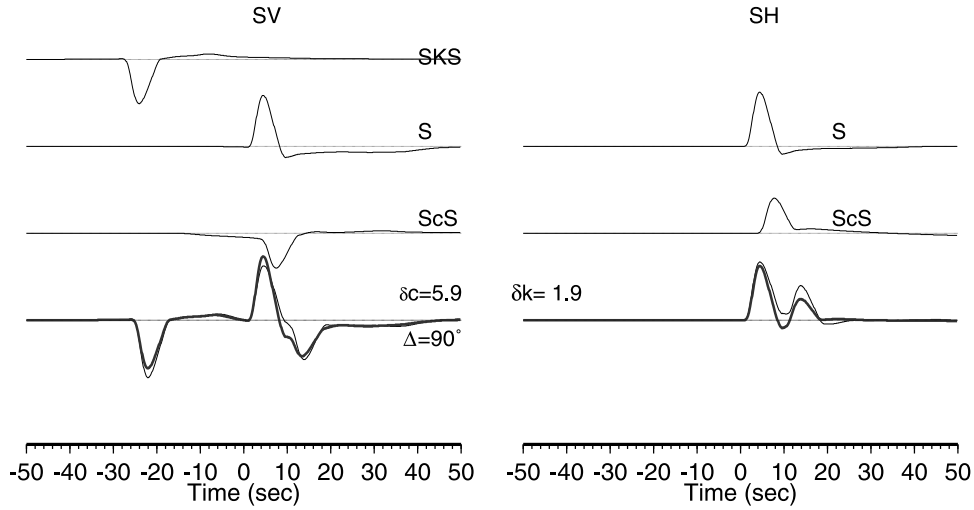

Figure 4. Presentation of the methodology used in calculating differential times of SKS-S and ScS-S. First, synthetic seismograms for SKS, S, and ScS are calculated for a 1-D reference model (PREM) as light traces (upper three). From the GRT point of view, these phases can be calculated separately by summing up responses of outer core rays, mantle rays, and the ray reflected from CMB respectively. Then the SKS synthetic and ScS synthetic are shifted (also with appropriate amplitude adjustment) with respect to S so as to obtain an optimal match with a test seismogram (bottom light traces). The numbers are time shifts of ScS (δc) and SKS (δk) required to match the test seismogram assumed to be that from the lower set of seismograms (LVZ). For this specific example, SKS is delayed 1.9 s and ScS is delayed 5.9 s, relative to S.

[6] In this paper, we apply the above procedure in two steps: (a) derive the timing shifts from data and comparing them with predictions from 2-D models; and (b) direct comparison of 2-D synthetics with observed data.

2. Differential Travel Time Analysis

[7] The interference of seismic arrivals is more common in crustal studies where different seismic arrivals have similar times. *Song and Helmberger* [1998] proposed a hybrid simulation method to study lateral variation in crustal velocities beneath southern California. Basically, they assume unperturbed seismic ray paths from a 1-D model, apply travel time corrections or shifts for the seismic phases, and then sum the shifted responses of each seismic phase to obtain a simulated seismogram. Observed waveforms along similar paths can then be matched and the shifts determined by simulated annealing to construct a 2-D tomography model [*Helmberger et al.*, 2001].

2.1. Algorithm and Testing

[8] Such concepts can be directly applied to teleseismic studies where interference of different arrivals are prominent (e.g., for the case of SKS and S crossover, and S and ScS emerging) because S, SKS and ScS are associated with distinct generalized ray paths: S is defined by all the rays in the mantle, not including the ray reflected from CMB, SKS is defined by all rays in the core, and ScS is defined by the ray reflected from CMB. To implement the hybrid-simulation technique, S, SKS and ScS groups are computed using the Cagniard de Hoop generalized ray theory (GRT) as discussed by *Helmberger* [1983] and displayed in Figure 3 for two models, PREM and a slow-basal layered model. We will attempt to use the PREM to generate individual phases and use them to simulate those from the slower model. Then each phase is shifted so as to obtain an optimal match with data by using a direct grid search. The procedure is displayed in Figure 4 where the various phases are assembled from Figure 3 (PREM). Note that ScS and S have the same polarity for SH component, and that SKS and ScS have opposite polarity from that of S on the SV component. Obviously, there is no SKS on SH component because of decoupling of P-SV and SH system assuming an isotropic Earth. By delaying SKS for 1.9 s and ScS for 5.9 s, the hybrid-simulated seismogram (HSS) matches the exact seismograms (heavy traces) closely.

[9] In Figure 5, the exact seismograms from GRT are compared to approximate seismograms. Most of the exact seismograms are matched by the approximated ones except for S and ScS phases beyond about 94° where diffraction

Table 1. Earthquakes Used in This Study

No.	Date	Time	Latitude, °	Longitude, °	Depth, km
1	20 October 1994	0115:16	−39.19	−70.80	164
2	19 August 1994	1002:51	−26.65	−63.38	565
3	29 July 1998	0714:24	−32.31	−71.29	51
4	2 September 1997	1213:22	3.85	−75.75	199
5	28 October 1997	0615:17	−4.37	−76.60	112
6	28 November 1997	2253:41	−13.74	−68.79	586
7	8 October 1998	0451:42	−16.12	−71.40	136
8	30 November 1999	0401:53	−18.78	−69.05	127
9	23 January 1997	0215:22	−22.00	−65.72	276
10	23 September 1995	2231:58	−10.53	−78.70	73
11	8 February 1995	1840:25	4.16	−76.64	69
12	15 October 1997	0103:33	−30.93	−71.22	58
13	3 April 1998	2201:48	−8.15	−74.24	164
14	3 April 1999	0617:18	−16.66	−72.66	87
15	25 May 1999	1642:05	−27.93	−66.93	169
16	14 February 1995	1553:56	−23.29	−67.70	156
17	12 December 1994	0741:55	−17.50	−69.65	151

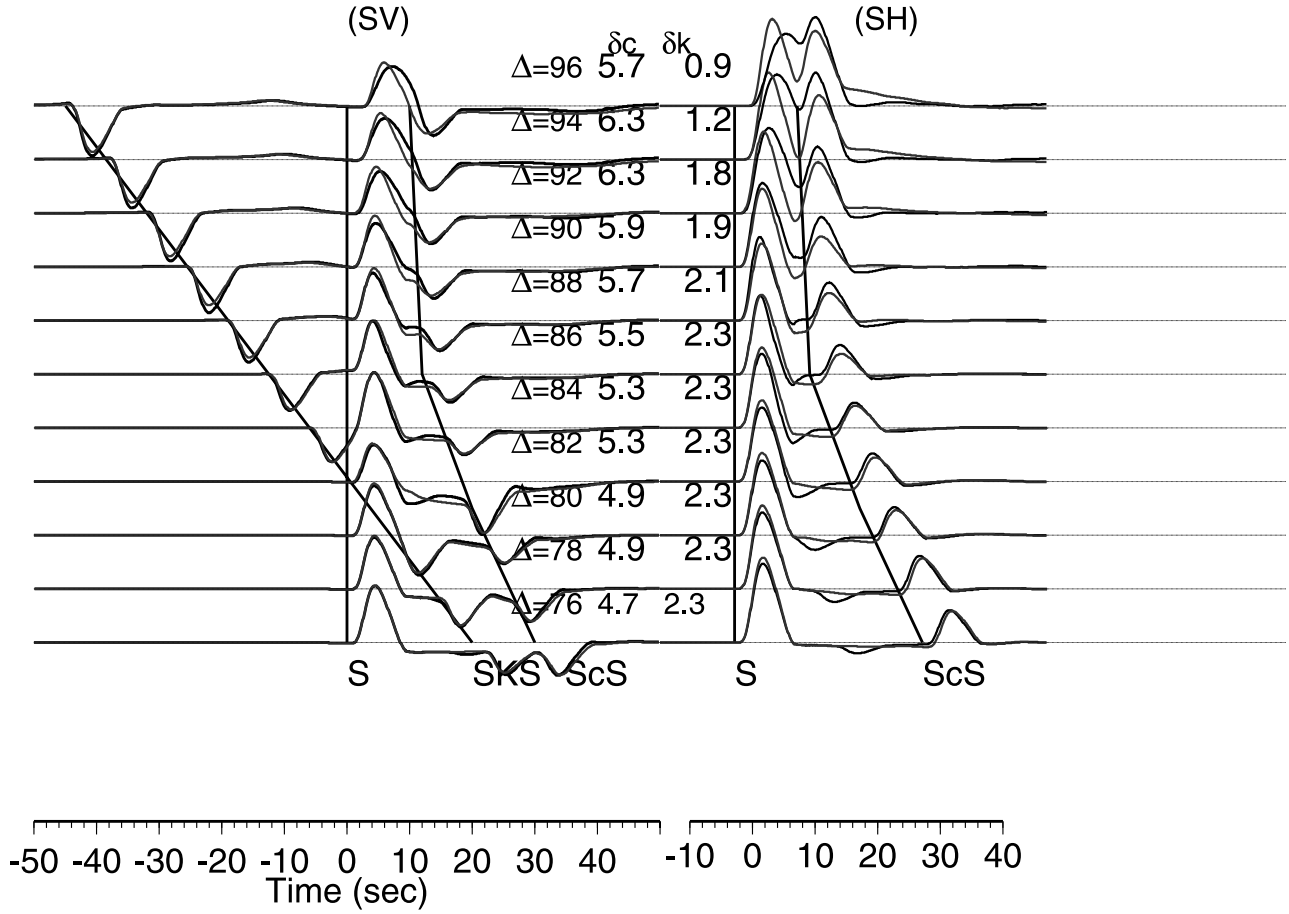
(SV)
(SH)
δc δk
Δ=96 5.7 0.9
Δ=94 6.3 1.2
Δ=92 6.3 1.8
Δ=90 5.9 1.9
Δ=88 5.7 2.1
Δ=86 5.5 2.3
Δ=84 5.3 2.3
Δ=82 5.3 2.3
Δ=80 4.9 2.3
Δ=78 4.9 2.3
Δ=76 4.7 2.3
S
SKS
ScS
S
ScS
-50 -40 -30 -20 -10 0 10 20 30 40
-10 0 10 20 30 40
Time (sec)

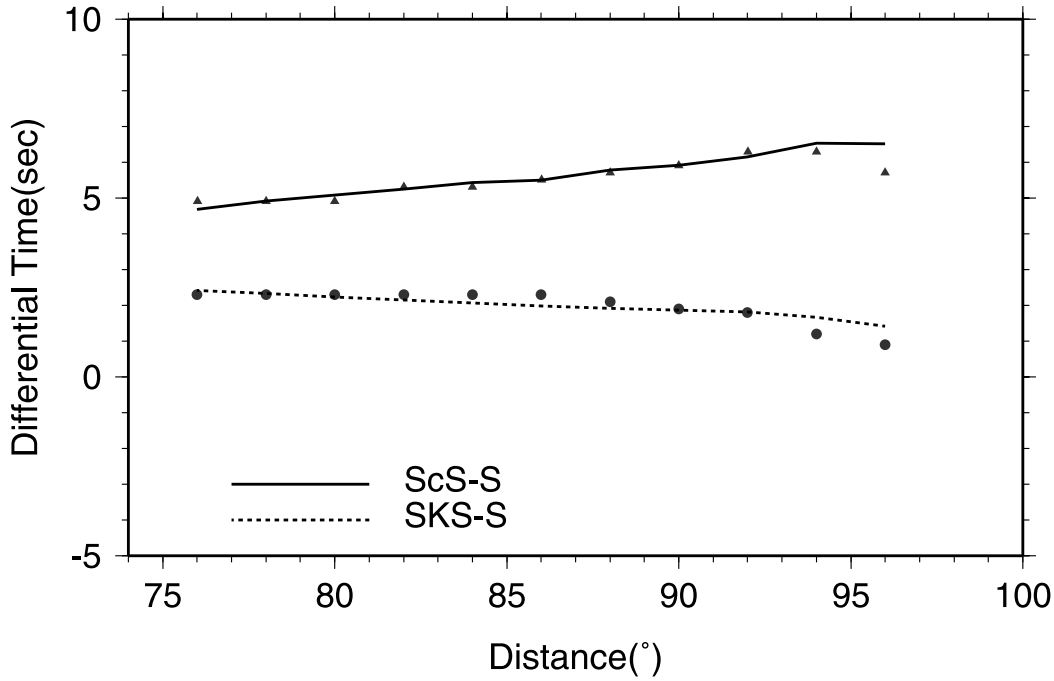
10
5
0
-5
Differential Time(sec)
ScS-S
SKS-S
75
80
85
90
95
100
Distance(˚)

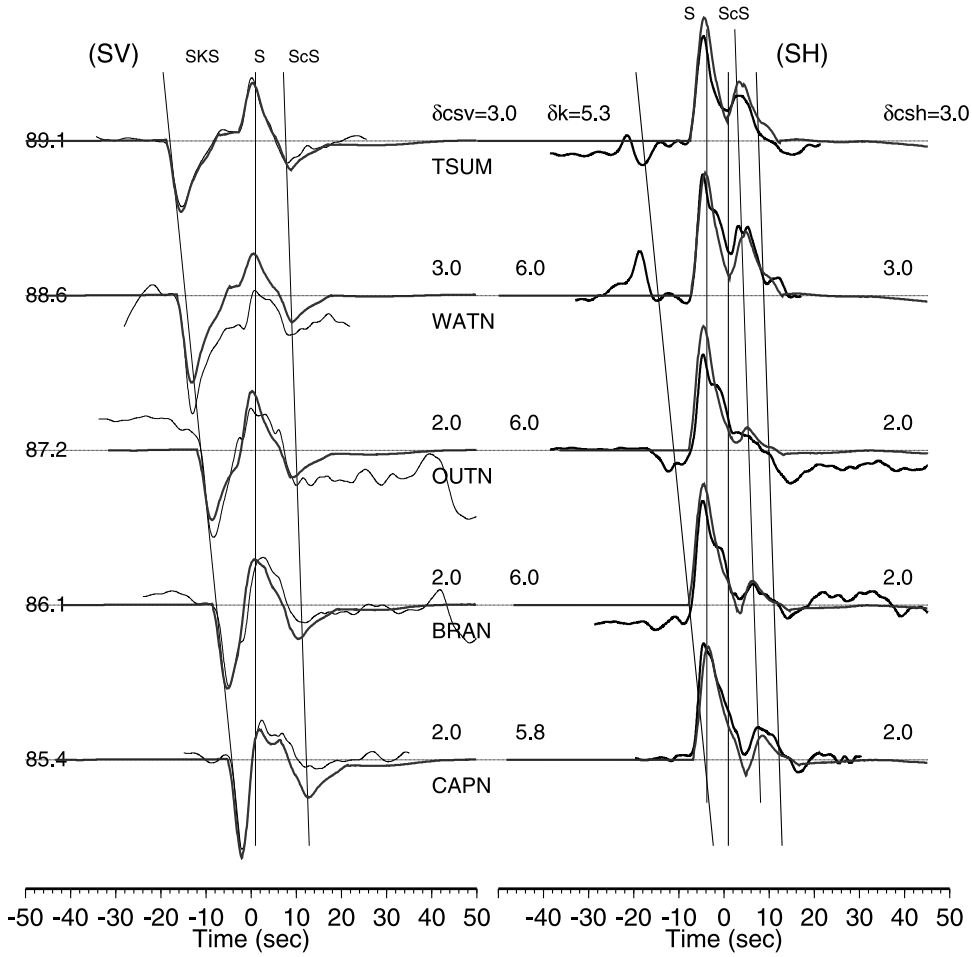

Figure 6. Record sections of simulated (light traces) and observed seismograms (heavy traces, for the radial (SV) and tangential (SH) components respectively) with epicentral distances given in degrees on the left. Note the large separations relative to PREM, where $\delta_k > \delta_c$ which is indicative of some vertical structure. The relative delays (ScS-S) for SV and SH are denoted by δ_{SV} and δ_{SH} which appear to be similar.

effects become more prominent. In these situations, the S ray paths begin to sample the low velocity layer, and the waveforms need to be modeled directly. In short, the differential times derived from HSS fit the theoretical calculation of differential times for the LVZ model quite well (lower panel) and prove useful in simulating effects produced by most velocity perturbations.

[10] The algorithm in its present form is used in an interactive mode where the researcher can view the waveform comparisons and choose the best lags, which are automatically stored as in tomographic routines [*Ritsema et al.*, 1999]. A similar procedure was used by *Lay and Young* [1990] in measuring SKS-S differential times.

2.2. Data and Analysis

[11] We applied this technique to African stations recording South American events at epicentral distances between 75° to 105°. The events (Table 1) and the stations we used are displayed in Figure 2. Only deep earthquakes (depth larger than 100 km) were used so that surface reflection phases will not contaminate the seismic phases we are interested in, and we used both IRIS broadband stations and WWSSN stations to study a corridor through the ALVS. Some South Africa PASSCAL array data presently being released are also included in this study. We only worked on high signal-to-noise ratio data where S, SKS, ScS are clear and no other processing procedures are applied other than standard processing to convert the velocity seismograms into displacement seismograms.

[12] The success in fitting seismograms with the HSS method suggests that our technique can be applied to the analysis of data routinely. The procedure works particularly well for arrays as displayed in Figure 6, where a record section of an earthquake recorded by Namibia array

Figure 5. (opposite) The upper panel displays a comparison of the LVZ seismograms displayed in Figure 3 (gray traces) with approximated seismograms (black traces) derived from the algorithm described in Figure 4. Typically, they agree well except for distances larger than 92° where diffraction effects become important. Note that δc is always larger than δk for slow-based layers due to geometry. The differential times of SKS-S and ScS-S obtained from HSS seismograms are plotted as dots (SKS-S) and triangles (ScS-S). They agree well with theoretical differential SKS-S (broken line) and ScS-S (solid line) in the lower panel. Beyond 90°, differential time of SKS-S and ScS-S decreases because S begins to be delayed due to the LVZ.

[*Hanka*, 1999, available at http://www.gfz-potsdam.de/geofon/namibia/] is analyzed. The SKS, S, and ScS phases are identified on each seismogram and the analysis of a record section helps to exclude the possibility of the wrong identification of seismic phases. Note that S and ScS have the same polarity on SH component while SKS and ScS have opposite polarity compared to S on the SV component. This polarity relationship makes identification of these three phases quite straightforward. Such a technique applied to high quality data typically yields a precision of about 0.3 s; it is hard to discern the difference between data and approximated seismogram if the specific phases are shifted by an amount smaller than 0.3 s. One complication might come from anisotropy in the upper mantle where SV seismograms have to be shifted in order to be aligned on SH phases. For the data set we processed, the misalignment of SV and SH components due to upper mantle anisotropy is less than 1 s, which agrees with upper mantle anisotropy study by *Silver et al.* [2001]. But upper mantle anisotropy should not change the differential times (SKS-S, SKS-ScS on the SV component) since on either component, each phase is affected identically due to the closeness of ray paths in the upper mantle. However, the anisotropy in the D″ region may affect the differential time between ScS and S. *Thomas and Heesom* [2000] showed that anisotropy is present in some fast D″ region based on high quality array data confirming earlier efforts by *Garnero and Lay* [1997]. The differential times between ScS and S on the SV component and on the SH appear to be similar (Figure 6) in this study. Thus we use ScS-S to denote the differential time between ScS and S in the remainder of this study. Note that this result is in agreement with recent studies beneath the Atlantic [*Fouch et al.*, 1999].

[13] The most obvious feature displayed in Figure 6 is the anomalously large separation between SKS and S of up to 6 s while the separation between ScS-S is about 3 s relative to PREM. This cannot be produced by a uniform basal layer as displayed in Figure 5 and indicates a slow structure along an isolated SKS path as suggested by *Ni et al.* [1999]. But since these paths are all sampling the middle of the ALVS (Figure 2), we do not see much variation. A clearer picture of the anomaly can be seen by examining the Tanzania Array data from the 20 October 1994 event (green paths) as displayed in Figure 2. In this case, the SKS essentially avoids the ALVS by arriving to the east of the structure. These data are displayed in Figure 7 along with an idealized 2-D model similar to that used by *Ritsema et al.* [1998a]. Note that the arrival time anomalies for S (Observation-PREM prediction) range up to 20 s although some of this delay is occurring just beneath the stations caused by the East African Rift Zone, i.e., *Ritsema et al.* [1998b]. This type of uncertainty can be avoided by fixing the station and studying an array of sources. Nevertheless, the delay of S

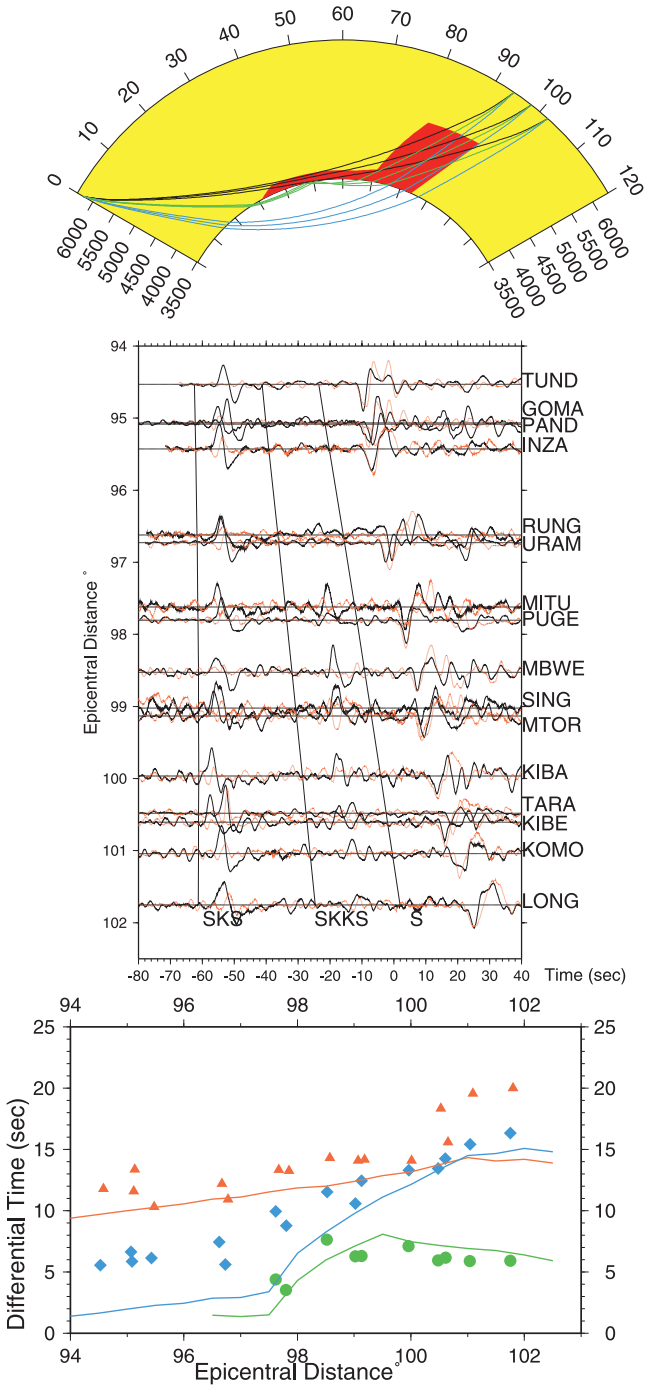

Figure 7. (opposite) The travel time constraints on the eastern edge of the ALVS from S, SKS, and SKKS observations. Ray paths of S (red), SKS (blue), SKKS (green), relative to ALVS are displayed at the top. The general feature is that S is delayed for all distances, but SKS begins to miss the structure around 98°. Predicted travel times for the model are given in the bottom panel (red line for S, green for SKKS-S and blue for S-SKS). Because SKS misses the ALVS around 98°, SKKS-SKS and S-SKSs times begin to increase rapidly with distance. The triangles, diamonds, and circles are observed S, S-SKS, SKKS-S time respectively derived from the data displayed in the middle panel where some SKS exit points are to the right of the EB boundary. The middle panel displays the observations with SV (dark) and SH (red). Stations TARA, KOMO, and LONG display the slowest S-wave arrivals relative to PREM related to the presence of the East-African Rift Zone. Note that the differential times reported by those three stations fall in the population. The SKS core exit points for these observations are given in Figure 2b.

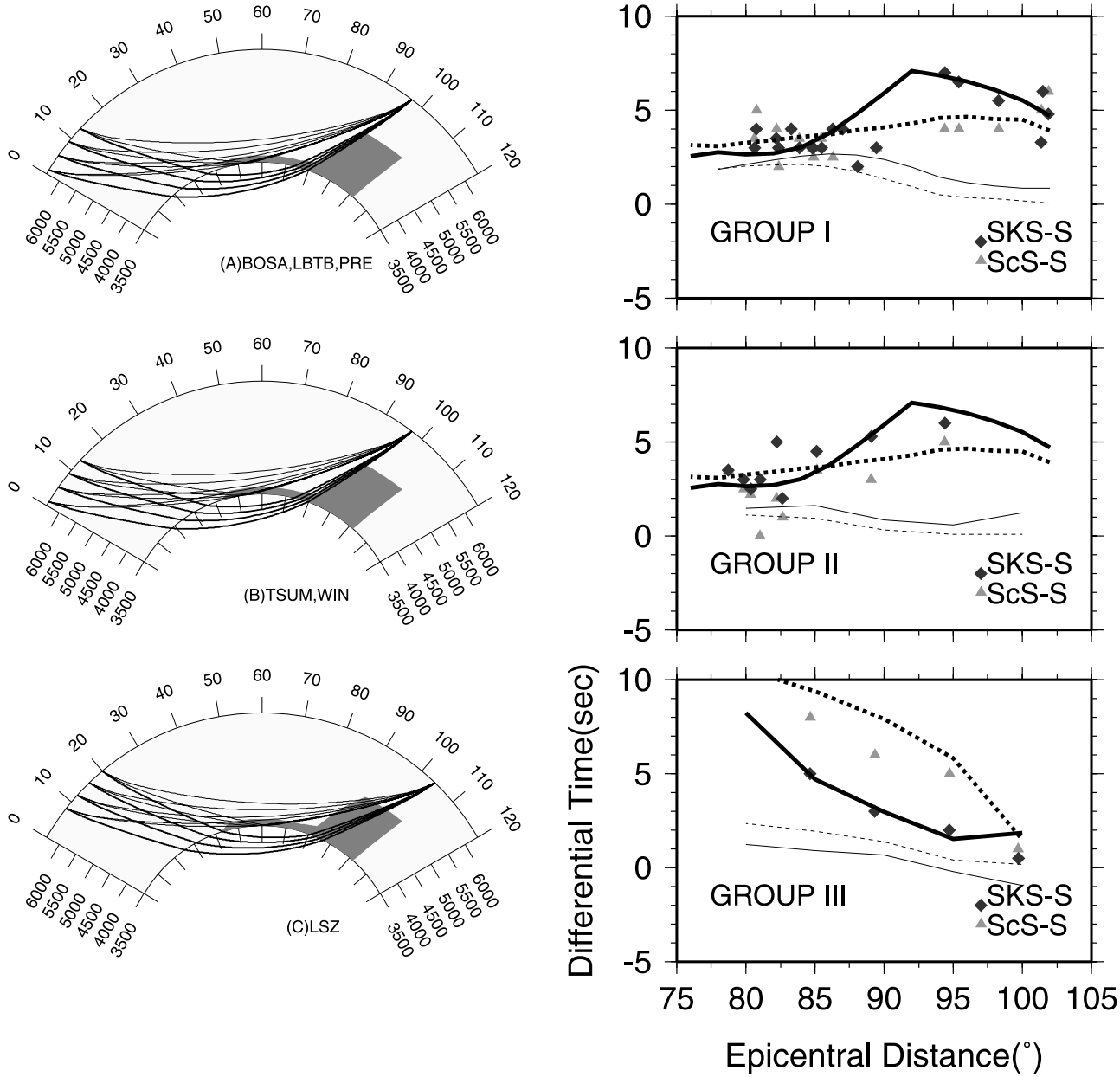

Figure 8. The three groups of differential time measurements (SKS-S, ScS-S) are displayed on the right. The pair of lines at the bottom of each panel is predicted from Ritsema's tomographic model. The solid line is the predicted SKS-S differential time from Ritsema's tomographic model, and broken line is the predicted ScS-S model. The upper set of thick lines are similar displays computed from the 2-D gray anomalous structure on the left. Travel time differentials obtained at the southern stations (A) are plotted in the upper-right panel (Group I), where the δ_k and δ_c times are nearly the same at ranges less than 85° which are easily explained with a simple basal layer, but not at the larger ranges. Similar results for stations (B) are plotted in the middle panel (Group II events). Results at LSZ are distinctly different as displayed in Group III, bottom right. The SKS exit points for these groups are displayed in Figure 2b (color coded).

relative to SKS reaching over 15 s is remarkable and must be caused predominantly by the deep mantle since the ray paths are quite similar near the receiver structure as displayed in Figure 1. SKKS is also delayed which can be explained by the upward portion of the path sampling the slow (red) structure.

[14] Next, we present results at fixed stations and examine an array of sources. Since some of the stations are near each other or have similar data properties, we have formed three groups: Group I contains the closely spaced stations BOSA, LBTB, and PRE (Figure 2). Stations GRM and SUR (located at south coasts of Africa) have only a few quality records and have been excluded, although considered in the earlier study of analog modeling, *Ni et al.* [1999]. Data from all these stations share similar trends. Their ScS bounce points are beneath the Atlantic, and their SKS exit points are

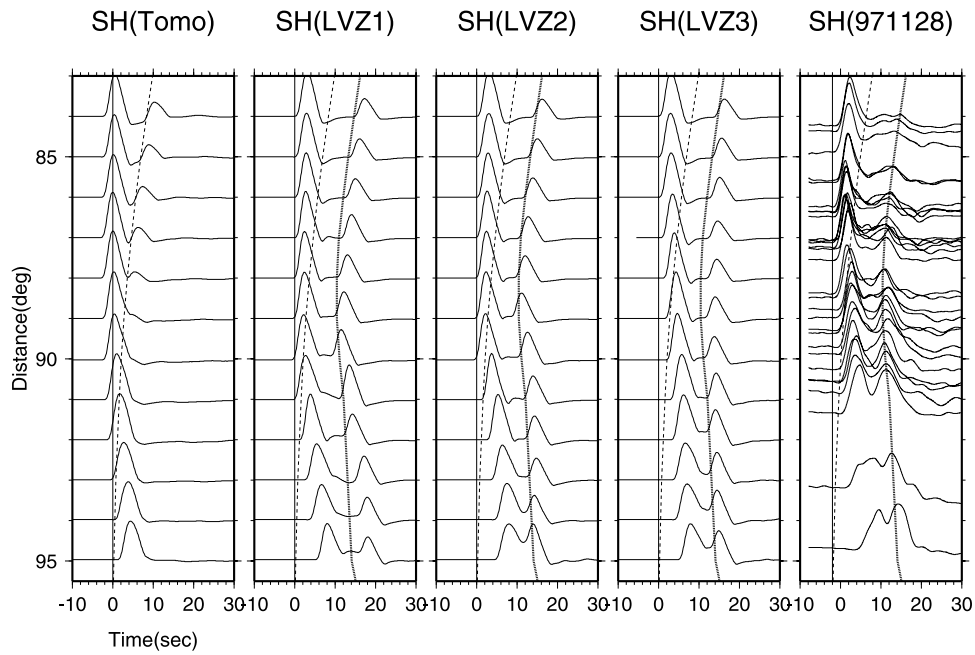

Figure 9. Data and 2-D synthetics *Ni et al.* [2000] for various models. Plots are aligned on the S arrival from PREM, with the broken line indicating the predicted ScS arrival. On the left (Tomo) synthetics based on Ritsema's model are displayed. The ScS is delayed about 3 s around 85°, but ScS and S are not separated after 90°. Synthetics for the other three hybrid models are plotted in the middle columns with the African array data (28 November 1997 event) on the right for comparison. We have included the reference lines from PREM (light and dashed) along with a heavy line indicating the observed ScS arrival.

near the WB (pink). Group II contains stations TSUM and WIN which sample paths at smaller latitudes but again have SKS exit points near the western boundary (Figure 2). Group III contains only the paths arriving at LSZ which have SKS points further toward the center of the ALVS. These paths are more unique and have been plotted in red.

[15] Tomographic predictions [*Ritsema et al.*, 1999] for the average (SKS-S) and (ScS-S) estimates for these three groups are displayed in Figure 8 along with the data. The predictions show only small deviations, which are commonly observed for long-period studies. For group I, the SKS-S points scatter about a delay of 2 to 4 s for ranges less than 90°. They increase to about 6 s beyond 95° with considerable scatter indicative of complex structure. These features can be explained by SKS encountering a slow structure (ALVS) as predicted by the red model. This same model explains the ScS-S delays, which are modest, at the 3 s level produced by the lower basal layer extending westward. A similar pattern exists for group II suggesting a NW trending ALVS with its western edge located roughly 15° westward of these two groups of stations, which is the ray offset between the surface and CMB exit points. Note that ScS samples only the western slow basal layer but does not cross any portion of the ALVS, as does the S phase. The (SKS-S) data from these two groups are quite similar but are more anomalous than (ScS-S) indicative of a delayed SKS as can be seen in the ray paths displayed. But for group III, the SKS-S and ScS-S decreases with larger epicentral distances, the explanation is that station LSZ is to the east of the western edge of the ALVS, and S ray paths begin to sample more of the ALVS with larger epicentral distances (steeper S ray paths), thus S is delayed more and more, causing smaller SKS-S and ScS-S time residuals relative to PREM. These features are fit by the travel times predicted from the 2-D structure as displayed. The low velocity layer beneath the Atlantic also separates ScS and S enough to be measured. It would not be possible to model ScS in this distance range for faster or normal D″ region where S and ScS are interfering. For ScS to be robust, the velocity structure close to the ScS bounce points must not contain substantial scatterers, which tend to diminish ScS [*Cormier*, 2000].

3. Waveform Constraints

[16] While the differential times assembled above are quite important in establishing a reliable model, they prove insufficient in number to generate a useful tomographic model. Thus we examined the synthetic predictions from a number of existing tomographic models to generate a working 2-D section. An example of such a synthetic record section generated from the model by *Ritsema et al.* [1999] was discussed earlier and repeated in Figure 9. The maximum delay of ScS relative to PREM is only 3 s, which is obviously insufficient to fit the data. However, the S-arrival delay with distance observed on synthetics shows the same general trend with S becoming delayed with range, roughly by 6 s as observed on data.

[17] The method of modifying tomographic models is similar to previous studies, *Ni et al.* [1999], which is basically to inflate velocity perturbations in the most sensitive zone so as to explain the large differential times.

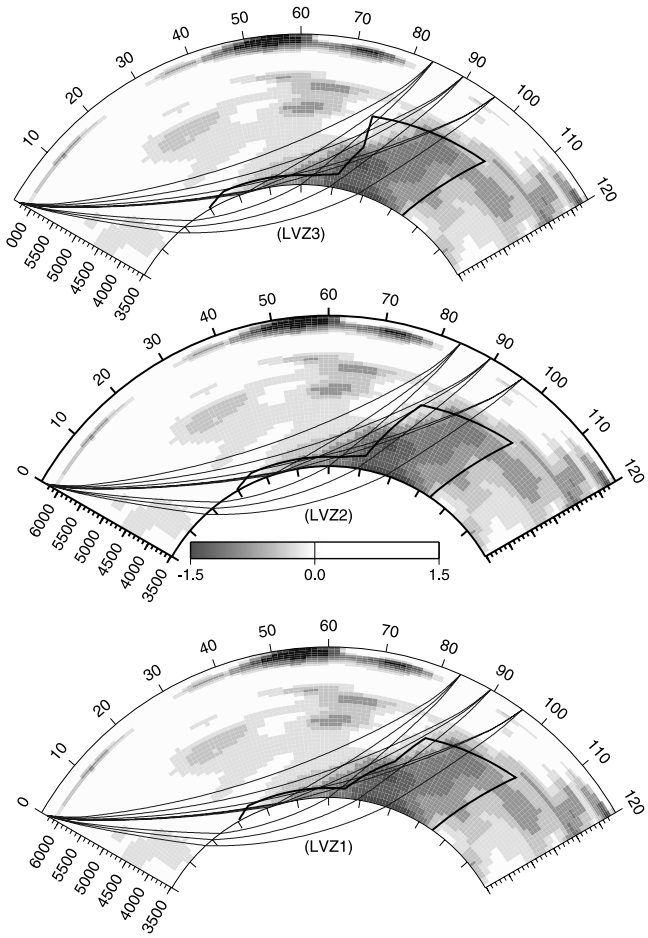

Figure 10. Ritsema's tomographic section along with three possible modifications given in black, from (13.8S,69.3W) to (28.5S, 25.8E). Ray paths of S, ScS, and SKS for epicentral distances of 84, 89, and 94° are displayed indicating the regions sampled by data from the South African array. Black lines are approximate contours that define the region of slow anomaly (3%) in the tomographic model. LVZ1 features a slow transition from a slow velocity layer to the large African upwelling while the transition in LVZ2 and LVZ3 are quite sharp. LVZ3 features more of a plume head type structure.

Three velocity models (Figure 10) were found to be generally compatible with the travel time data. The background model is Ritsema's model, with maximum velocity anomaly of about 1.5%, and the average is about 1%. We developed the three models by drawing a contour that defines the low velocity region (the black line), and we set the velocity perturbation to be 3% slower in the region enclosed by the black lines. Given the diffused nature of the tomographic models, the edge of the low velocity region is not well defined. We attempted to model the edge with LVZ1 containing a relatively slow transition from low velocity layer while the transition in model LVZ2 and LVZ3 is sharper. Note that the LVZ2 model is simply the ALVS (gray model in Figure 8) structure overlaying the tomographic model. The difference between LVZ2 and LVZ3 is that the latter has more of a plume head structure.

[18] We computed 2-D synthetic seismograms (Figure 9) for the original tomographic model (Ritsema) and the three variant models. For the unenhanced tomographic model, the ScS are delayed about 3 s around 85° which is expected since it is constrained with ScS data for epicentral distances less than about 85°. But for larger epicentral distances, the S and ScS essentially becomes one pulse in the synthetics, and this does not agree with the data, which shows large separations between S and ScS up to 95°. For the three

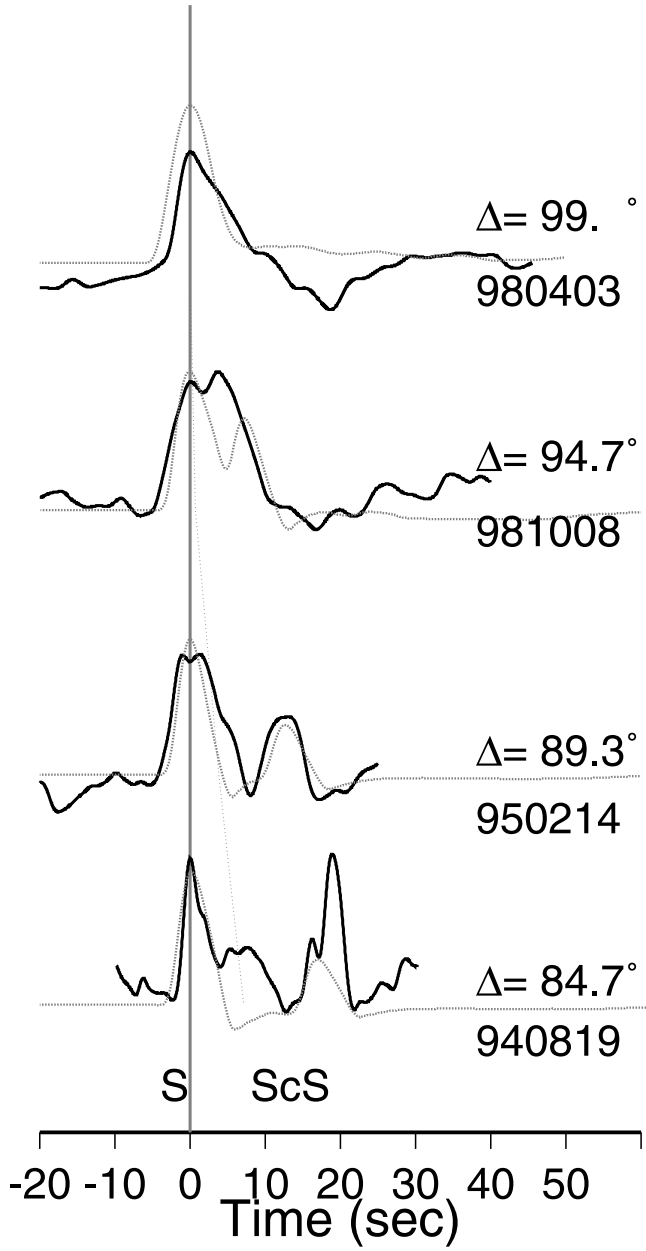

Figure 11. Comparison of data (heavy traces) at LSZ and synthetics (light traces) for model LVZ2. All traces are aligned on the S arrival with the curve denoting ScS-S differential time for PREM indicated as a dashed line. It is obvious that ScS is very delayed (with respect to S) around 85°; but it is close to S around 100°. The only way to separate S and ScS beyond about 100° is to introduce a ULVZ as discussed by *Ni and Helmberger* [2001] and *Wen et al.* [2001].

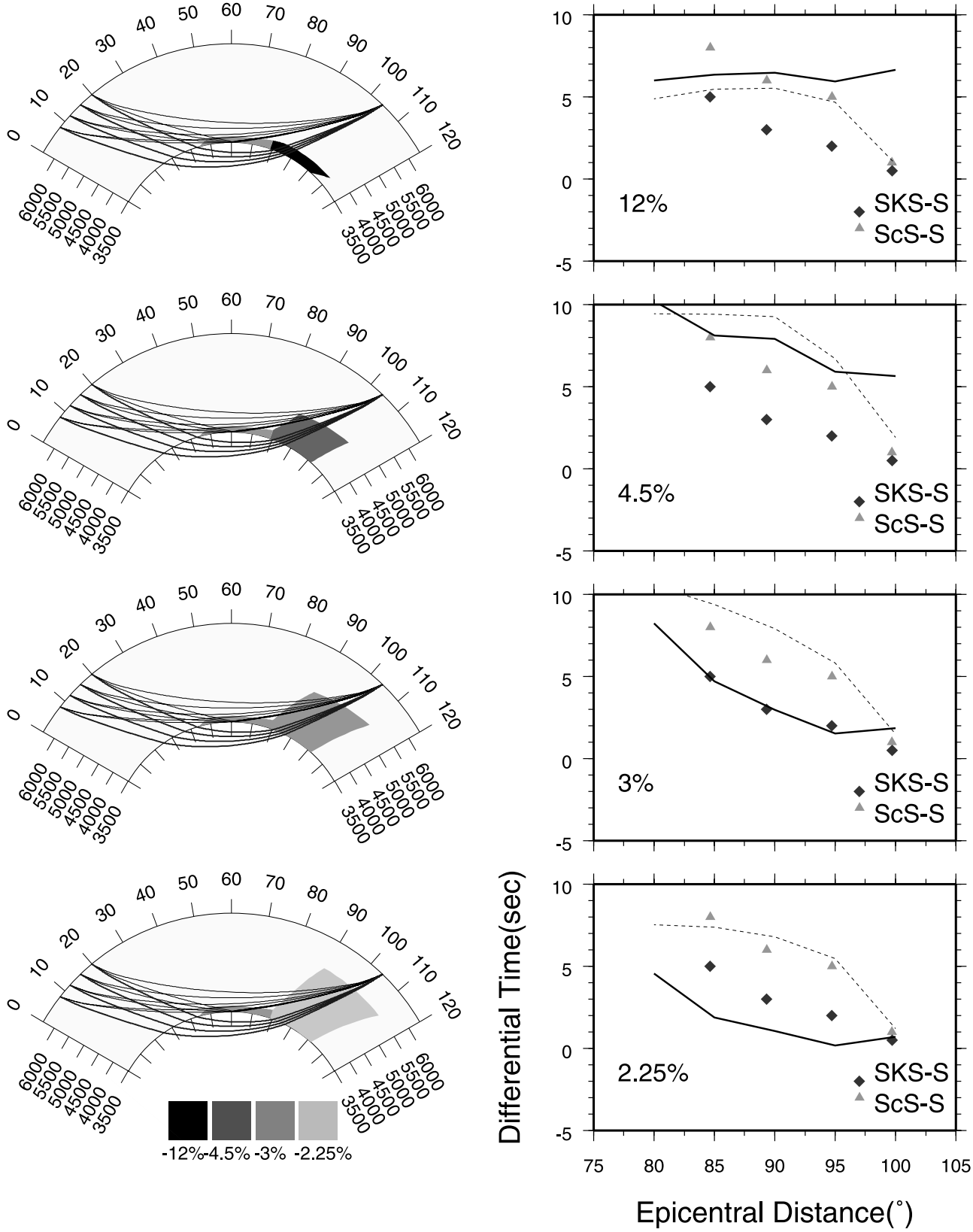

Figure 12. ALVS thickness sensitivity testing. Cross-sections with various thickness are presented on the left along with ray paths where the travel times of SKS have been preserved. The basal layer on the left (D″ beneath the Atlantic) is maintained at 3%. The ALVS thickness varies from 300, 1000, 1500, and 2000 km, with velocities reductions at 12% to 2.25%. The associated differential travel time predictions (SKS-S) and (ScS-S) are displayed on the right along with the data for Group III.

enhanced models, ScS are always delayed due to the low velocity layers. However, for model LVZ1, the ScS phase samples an effectively thicker low velocity layer at ranges >92°, thus ScS is delayed too much as compared to the data. With the sharp transition, synthetics for model LVZ2 and LVZ3 both fit the data quite well, and this is reasonable since the S and ScS ray paths in the upper mantle where the plume head is located are very close together. While LVZ2 fits the waveform data quite well at distances beyond 87°, there is a noticeable mismatch at shorter distances as discussed earlier.

[19] The sharp transition in LVZ2 needed to fit the waveform data is also favored by differential travel time data as displayed earlier in Figure 8. Note that the predicted differential travel times from model LVZ2 are overlaid with observed data and fit fairly well for groups I and II. One noticeable feature for group (III) (station LSZ) is that model LVZ2 predicts decreased SKS-S and ScS-S just as the data shows, and the predicted S travel time is increasingly delayed because the S ray path does not sample the ALVS for small epicentral distances, and S ray path samples a larger and larger portion of the ALVS with increasing distances. Events from Sandwich Island recorded at LSZ (epicentral distance about 60°) show very delayed ScS (up to 12 s), and this also supports the idea that ray paths with small takeoff angle sample the bulk of the low velocity anomaly. A record section of synthetic seismograms for sources at different distances from station LSZ is compared to data in Figure 11. The large separation of ScS and S at the distance of about 85° and the diminishing separation around 100° is reproduced by synthetics. Thus, model LVZ2 can explain a record section of data with a fixed source and varying stations and a record section of data with fixed station and varying sources. This combination of data helps eliminate shallow structural problems such as those occurring beneath the Tanzania Array [*Ritsema et al.*, 1998b].

4. Discussion and Conclusion

[20] Generally, there is the problem of uniqueness associated with forward modeling. We discuss this issue by analyzing the differential travel times of SKS-S and ScS-S for a series of models with varying thickness. For station LBTB and TSUM, only SKS ray paths sample the slow portion of the structure as discussed earlier and the uniqueness cannot be well resolved since SKS ray paths are quite steep. The geometry of S, ScS, and SKS ray paths for station LSZ is ideal to address the uniqueness problem because S and ScS ray paths begin to sample the slow region with increasing epicentral distances. We select four representative models (Figure 12), with the heights constrained at 2000 km, 1500 km, 1000 km and 300 km. The velocity reduction within the upwelling region is 2.25%, 3%, 4.5%, and 12% respectively, so as to keep SKS uniformly delayed as expected from LBTB and TSUM data (Figure 8). S is delayed too much for the 2000 case thus SKS-S is too small as compared with data. But with the thinner structures (1000 km to 300 km), SKS-S is too large because S ray paths do not sample the slow region. The differential time of ScS-S can also provide some constraints on the size of the upwelling structure but it is not as powerful as differential times of SKS-S because the ray paths of S and ScS are much closer to each other than the ray paths of SKS and S. Based on the analysis of these four models, it seems that the ALVS extends upward between 1000 km and 2000 km above the CMB and a height of 1500 km with velocity contrast of 3% relative to velocities outside the structure can fit most data sets. Another concern is the 3-D effects on the seismic waveforms since the ALVS is obviously 3-D given its ridge-like nature as shown in Figure 2b. Seismic rays could well deviate from the great circle plane because of ray bending due to rapid lateral variation. However, for the current waveform modeling, the great circle ray path is almost perpendicular to the strike of the ridge, thus 2-D modeling should be able to account for majority of waveform distortions.

[21] The sharpness issue is more difficult to quantify, especially when working with an array of sources with their origin time and waveform uncertainties. These problems can be eliminated when array data exist as displayed in Figure 7. Unfortunately for our purposes, this array was situated across the East African Rift Zone. Stations at smaller ranges are in the craton region and show about a 5 s delay for SKS relative to PREM. When the travel times for the whole array are corrected for upper mantle structure, *Ritsema et al.* [1998a], one sees about a 5 s jump from late to normal at about 98°. Several SKS waveforms near this jump are fat, i.e., MBWE, which can be explained by multipathing. A sensitivity study indicates a relatively sharp boundary with a transition thickness of less than 60 km in this sample. SKS results from the South African Array are easier to analyze because of the uniformity of local upper mantle structure. Many events display even larger abrupt jumps in SKS when crossing the EB edge [*Ni et al.*, 2002].

[22] In conclusion, we have developed an algorithm to measure the differential times between interfering phases such as SKS, S, and ScS by waveform matching. Application of the technique to data obtained along the South American-African corridor reveals large differential anomalies relative to PREM. We have used these travel time residuals in conjunction with a 2-D waveform modeling technique to construct a detailed 2-D shear velocity section through the great ALVS. Our model features a relatively flat low velocity layer (3% slower in S velocity, 200 km thick) beneath the Atlantic, that transitions into the African ridge like structure with a width of about 1000 km and extending upward 1200 km above the CMB. The transition is relatively sharp, which is required by S and ScS waveforms recorded by the South Africa array. Such a sharp transition agrees with cross-sections from other studies [*Ritsema et al.*, 1998a; *Ni et al.*, 1999] based on different data sets. Some geodynamic simulations produce such large-scale structures with particularly strong temperature viscosity dependence [*Thompson and Tackley*, 1998; *Bergeron et al.*, 2000; *Tan et al.*, 2002], but it remains difficult to explain the sharp lateral boundaries presented in our simplified structures without some chemical effects. Such detailed images will be examined more closely in a subsequent effort.

[23] **Acknowledgments.** Thanks to the IRIS DMC and GEOFON program for providing digital waveform data, and for the useful comments from Thorne Lay, Associate Editor and an anonymous reviewer. This research is supported by NSF grant EAR-9629279. Contribution 8836 of

the Division of Geological and Planetary Sciences, California Institute of Technology.

References

Bergeron, S., D. A. Yuen, and A. P. Vincent, Capabilities of 3-d wavelet transforms to detect plume-like structures from seismic tomography, *Geophys. Res. Lett.*, *27*, 3433–3436, 2000.

Cormier, V. F., D″ as a transition in the heterogeneity spectrum of the lowermost mantle, *J. Geophys. Res.*, *105*, 16,193–16,205, 2000.

Dziewonski, A. M., and D. L. Anderson, Preliminary reference Earth model, *Phys. Earth Planet. Inter.*, *25*, 297, 1981.

Fouch, M. J., P. G. Silver, and D. E. James, Probing for shear wave anisotropy in the lowermost mantle beneath and Atlantic and Indian Oceans, *Eos Trans. AGU*, *80*(46), Fall Meet Supl. Abstract S52A-19, 1999.

Garnero, E., and T. Lay, Lateral variations in lowermost mantle shear wave anisotropy beneath the North Pacific and Alaska, *J. Geophys. Res.*, *102*, 8121–8135, 1997.

Grand, S. P., Mantle shear structure beneath the Americas and surrounding oceans, *J. Geophys. Res.*, *99*, 11,591–11,622, 1994.

Gurnis, M., J. X. Mitrovica, J. Ritsema, and H. Van Heijst, Constraining mantle density structure using geological evidence of surface uplift rates: The case of the African super plume, *Geochem. Geophys. Geosyst.*, *1*, 35, 2000.

Hager, B. H., R. W. Clayton, M. A. Richards, R. P. Comer, and A. M. Dziewonski, Lower mantle heterogeneity; dynamic topography and the geoid, *Nature*, *313*, 541–545, 1985.

Hanka, W., Broadband seismological experiment in Namibia, 1999.

Helmberger, D. V., Theory and application of synthetic seismograms, in *Earthquakes: Observation, Theory, and Interpretation*, vol. 37, Italian Physical Society (Enrico Fermi), edited by H. Kanamori and E. Boschi, pp. 174–217, North-Holland, New York, 1983.

Helmberger, D. V., X. Song, and L. Zhu, Crustal structure beneath southern California from waveform modeling, *J. Geophys. Res.*, *106*, 609–620, 2001.

Lay, T., and C. J. Young, The stably-stratified outermost core revisited, *Geophys. Res. Lett.*, *17*, 2001–2004, 1990.

Li, X.-D., and B. Romanowicz, Global mantle shear velocity model developed using nonlinear asymptotic coupling theory, *J. Geophys. Res.*, *101*, 22, 1996.

Luo, S., S. Ni, and D. Helmberger, Ultra low velocity zone revealed from multipathed PKPab, *Earth Planet. Sci. Lett.*, *189*, 155–164, 2001.

Masters, T. G., S. Johnson, G. Laske, and H. Bolton, A shear-velocity model of the mantle, *Philos. Trans. R. Soc. London*, *354*, 1385–1411, 1996.

Ni, S., and D. V. Helmberger, Horizontal transition from fast (slab) to slow (plume) structures at the core-mantle boundary, *Earth Planet. Sci. Lett.*, *187*, 301–310, 2001.

Ni, S., X. Ding, and D. V. Helmberger, Low velocity structure beneath Africa from forward modeling, *Earth Planet. Sci. Lett.*, *170*, 497–507, 1999.

Ni, S., X. Ding, and D. V. Helmberger, Constructing synthetics from deep earth tomographic models, *Geophys. J. Int.*, *140*, 71–82, 2000.

Ni, S., E. Tan, M. Gurnis, and D. V. Helmberger, Sharp sides to the African super plume, *Science*, *296*, 1850–1852, 2002.

Ritsema, J., S. Ni, D. V. Helmberger, and H. P. Crotwell, Evidence for strong shear velocity reductions and velocity gradients in the lower mantle beneath Africa, *Geophys. Res. Lett.*, *25*, 4245–4248, 1998a.

Ritsema, J., A. Nyblade, T. J. Owens, C. A. Langston, and J. C. VanDecar, Upper mantle seismic velocity structure beneath Tanzania, *J. Geophys. Res.*, *103*, 21,201–21,213, 1998b.

Ritsema, J., H. Van Heijst, and J. Woodhouse, Complex shear wave velocity structure imaged beneath Africa and Iceland, *Science*, *286*, 1925–1928, 1999.

Silver, P. G., S. Gao Liu, and H. Kelly, Mantle deformation beneath Southern Africa, *Geophys. Res. Lett.*, *28*, 2493–2496, 2001.

Song, X., and D. Helmberger, Pseudo Green's functions and waveform tomography, *Bull. Seismol. Soc. Am.*, *88*, 304–312, 1998.

Su, W.-J., R. L. Woodward, and A. M. Dziewonski, Degree 12 model of shear velocity heterogeneity in the mantle, *J. Geophys. Res.*, *99*, 6945–6980, 1992.

Tan, E., M. Gurnis, and L. Han, Slabs in the lower mantle and their modulation of plume formation, *Geochem. Geophys. Geosyst.*, 3(11), 1067, doi:10.1029/2001GC000238, 2002.

Thomas, C., and T. Heesom, Comparisons of D″ anisotropy in three different regions, in *SEDI Proceedings*, p. 53, Study of the Earth's Deep Interior, 2000.

Thompson, P. F., and P. J. Tackley, Generation of mega-plumes from the core-mantle boundary in a compressible mantle with temperature-dependent viscosity, *Geophys. Res. Lett.*, *25*, 1999–2002, 1998.

Wen, L., P. Silver, D. James, and R. Kuehnel, Seismic evidence for a thermo-chemical boundary at the base of the Earth's mantle, *Earth Planet. Sci. Lett.*, *189*, 141–153, 2001.

S. Ni and D. V. Helmberger, Seismological Laboratory, California Institute of Technology, Pasadena, CA 91125, USA. (stone@gps.caltech.edu)